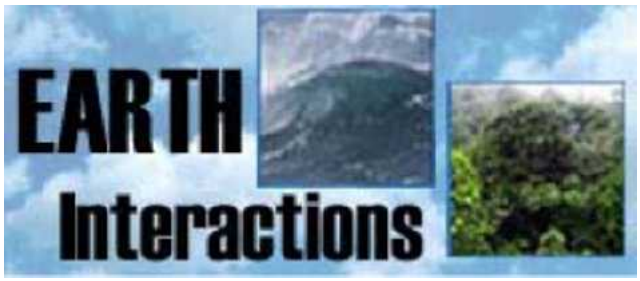

Global Biomass Variation and Its Geodynamic Effects: 1982–98

M. Rodell*

Hydrological Sciences Branch, NASA Goddard Space Flight Center, Greenbelt, Maryland

B. F. Chao

Space Geodesy Branch, NASA Goddard Space Flight Center, Greenbelt, Maryland

A. Y. Au

Raytheon ITSS, and Space Geodesy Branch, NASA Goddard Space Flight Center, Greenbelt, Maryland

J. S. Kimball

University of Montana, Flathead Lake Biological Station, Polson, Montana

K. C. McDonald

Terrestrial Science Research Element, NASA Jet Propulsion Laboratory, Pasadena, California

Received 1 September 2004; accepted 28 December 2004

ABSTRACT: Redistribution of mass near Earth's surface alters its rotation, gravity field, and geocenter location. Advanced techniques for measuring these geodetic variations now exist, but the ability to attribute the observed modes to individual Earth system processes has been hampered by a shortage of reliable

* Corresponding author address: M. Rodell, Hydrological Sciences Branch, NASA Goddard Space Flight Center, Code 614.3, Greenbelt, MD 20771.
E-mail address: Matthew.Rodell@nasa.gov

global data on such processes, especially hydrospheric processes. To address one aspect of this deficiency, 17 yr of monthly, global maps of vegetation biomass were produced by applying field-based relationships to satellite-derived vegetation type and leaf area index. The seasonal variability of biomass was estimated to be as large as 5 kg m^{-2}. Of this amount, approximately 4 kg m^{-2} is due to vegetation water storage variations. The time series of maps was used to compute geodetic anomalies, which were then compared with existing geodetic observations as well as the estimated measurement sensitivity of the Gravity Recovery and Climate Experiment (GRACE). For gravity, the seasonal amplitude of biomass variations may be just within GRACE's limits of detectability, but it is still an order of magnitude smaller than current observation uncertainty using the satellite-laser-ranging technique. The contribution of total biomass variations to seasonal polar motion amplitude is detectable in today's measurement, but it is obscured by contributions from various other sources, some of which are two orders of magnitude larger. The influence on the length of day is below current limits of detectability. Although the nonseasonal geodynamic signals show clear interannual variability, they are too small to be detected.

KEYWORDS: Biogeochemical cycles, Earth rotation variations, Time-variable gravity, Remote sensing

1. Introduction

A great quantity of mass, on the order of 1 teraton (10^{15} kg; equivalent to 1000 km^3 of water), is sequestered in the body of living organisms as biomass. The majority of global biomass exists as vegetation, which covers much of the land surface. Vegetation density is highly variable geographically, but it also varies in time. It undergoes large seasonal variations, including the emergence and shedding/drying of leaves of deciduous trees in the vast temperate zones, the crop cycles in agricultural land, and the seasonal growth and disappearance of opportunistic plants in the Arctic. It also undergoes interannual variations dependent upon land use and climate variability.

Temporal variations of biomass distribution were computed and are presented below for 17 yr from which consistent satellite observations of vegetation properties are available. The resultant global geodynamic effects were quantified and compared against geodetic observations, for both seasonal and interannual signals. In accounting for the destination of the water involved it was assumed that plants exchange water from their land location ultimately with the (uniform) ocean as source and sink. There are also biomass variations in the ocean itself, but the mass is floating and thus inseparable from ocean water mass, so these were not considered here.

The geodynamic effects of mass transport in the Earth system include variations in Earth's rotation (e.g., Gross 2000), gravity field (e.g., Nerem et al. 1993), and geocenter (e.g., Chao et al. 2000; see Table 1). Although relatively tiny, these variations have been observed using highly precise modern space geodetic techniques (Smith and Turcotte 1993). What is observed is the total effect of redistributions of all forms of mass, including those that occur near Earth's surface in the atmosphere, hydrosphere, and cryosphere (e.g., Kuehne and Wilson 1991).

Table 1. Global geodynamic effects of mass transport in the Earth system.

Geodynamic effect	Physical principle	Geodetic parameters	Remarks
Time-variable gravity	Newton's gravitational law	(Spherical harmonic) Stokes coefficients	All degrees and orders
Earth's rotation variation	Conservation of angular momentum	Polar motion, LOD	"Mass term" related to second-degree (order = 0,1) Stokes coefficients
Geocenter motion	Conservation of linear momentum	(3D) Geocenter vector	Related to first-degree Stokes coefficients

These mass variations predominate on daily to interannual time scales, superimposed upon those in the solid Earth, which are generally greater in magnitude but far longer in time scale.

The aforementioned mass variability includes that of the global biomass. To be sure, the contribution of biomass, which for the purposes of this research may be considered part of the hydrosphere, is relatively small simply by virtue of the relatively small amount of total mass involved. However, as biomass variability has begun to be assessed on a global scale using modern remote sensing and modeling techniques, its contributions to global geodynamics can now be isolated and identified. The significance of the latter is twofold, as described next.

Historically, the effect of biomass variations on Earth's rotation was first raised and documented by Jeffreys (Jeffreys 1916), tracing back to Sir Harold's earlier career as a botanist. According to Jeffreys:

> "During the summer the vegetative parts of plants increase in mass in two ways. In trees, large quantities of sap rise from the ground, and thus the woody parts become heavier. Leaves are also produced in deciduous trees. In herbs, the whole of the subaerial portion is regenerated annually in the earlier part of the summer. Later in the year, usually in late summer or early autumn, the subaerial parts of all terrestrial plants partially dry up, and ultimately herbs wilt and fall to the ground, while deciduous trees cast all their leaves. The dead portions continue to lose weight until decomposition is complete. We may say then that there is a periodic part of the mass of trees, shrubs, and herbs which has a maximum in summer and a minimum in winter."

Jeffreys (Jeffreys 1916) came up with an estimate of 33 kg m^{-2} for the maximum seasonal amplitude of biomass density at high latitudes, and nearly 10 milliarcseconds (mas) for the biomass excitation of polar motion, which is a gross overestimate (see below). Munk and MacDonald (Munk and MacDonald 1960) also pondered the subject; they gave an estimate about 7 times smaller based on Riley's (Riley 1944) assessment of the annual production of organic carbon on land, corresponding to no more than 1 mas of polar motion excitation. Below we provide presumably a more definitive answer to this age-old question based on modern knowledge; our result yields estimates yet another order of magnitude smaller.

On the other hand, and perhaps more importantly, the new Gravity Recovery and Climate Experiment (GRACE) satellite mission is now providing accurate,

high-resolution measurements of Earth's time-variable gravity field (Tapley et al. 2004a). To use such data to quantify mass variability in the Earth system (as GRACE hopes to do), one should strive to account for all known contributions. Over land, the contributions of soil moisture, groundwater, and snow mass variability each can be substantial, but the magnitudes of mass variations in other hydrological components, including biomass, are not well known (Rodell and Famiglietti 2001). It is shown below that the seasonal biomass contribution to time-variable gravity is nonnegligible. The geocenter motion caused by the biomass's seasonal-hemispherical mass shift is similar. Monitoring the geocenter is of central importance in the ever-evolving definition of our terrestrial reference frame.

2. Biomass distribution: 1982–98

Although accurate measurements of biomass can be made in situ, remote sensing is the only hope for monitoring biomass distribution globally. Two satellite-based remote sensors, the Advanced Very High Resolution Radiometer (AVHRR) and the Moderate Resolution Imaging Spectroradiometer (MODIS), have provided measurements at the electromagnetic wavelengths necessary for estimating certain vegetation characteristics. In particular, global maps of vegetation type and leaf area index (LAI; i.e., the average leaf area per unit land surface area) are now being retrieved. For consistency in this study, only the AVHRR data were used. A monthly time series of biomass distribution was generated using a vegetation classification dataset, maps of LAI, and a land-cover-based index of general allometric relationships between LAI and foliar and stem biomass derived from field observations.

Hansen et al. (Hansen et al. 2000) produced the global land-cover dataset used here based on observations from the National Oceanic and Atmospheric Administration (*NOAA-15*) satellite's AVHRR system (Figure 1). This dataset assigns the land cover in each 1-km pixel to 1 of 14 types: 1) water, 2) evergreen needle-leaf forest, 3) evergreen broadleaf forest, 4) deciduous needle-leaf forest, 5) deciduous broadleaf forest, 6) mixed forest, 7) woodland (40%–60% tree cover), 8) wooded grassland (10%–40% tree cover), 9) closed shrubland (>40% shrub cover), 10) open shrubland (10%–40% shrub cover), 11) grassland and cereal crops, 12) broadleaf crops, 13) barren or ice covered, and 14) urban.

Monthly LAI fields were derived at Boston University using the algorithm of Myneni et al. (Myneni et al. 1997) and Nemani and Running (Nemani and Running 1997) for the period from January 1982 to December 1998 from AVHRR measurements of the normalized difference vegetation index (NDVI) and other satellite observations. These were scaled from 8- down to 1-km resolution, to match the land-cover dataset, using information from that dataset and known relationships between NDVI and LAI (J. Dong, University of Maryland Baltimore County, 2003, personal communication). Annual maximum and minimum LAI values were then extracted on a pixel-by-pixel basis from the monthly LAI maps.

The following set of equations was used to compute the total biomass (TB) within each 1-km pixel, and the results were then averaged up to 1° spatial resolution:

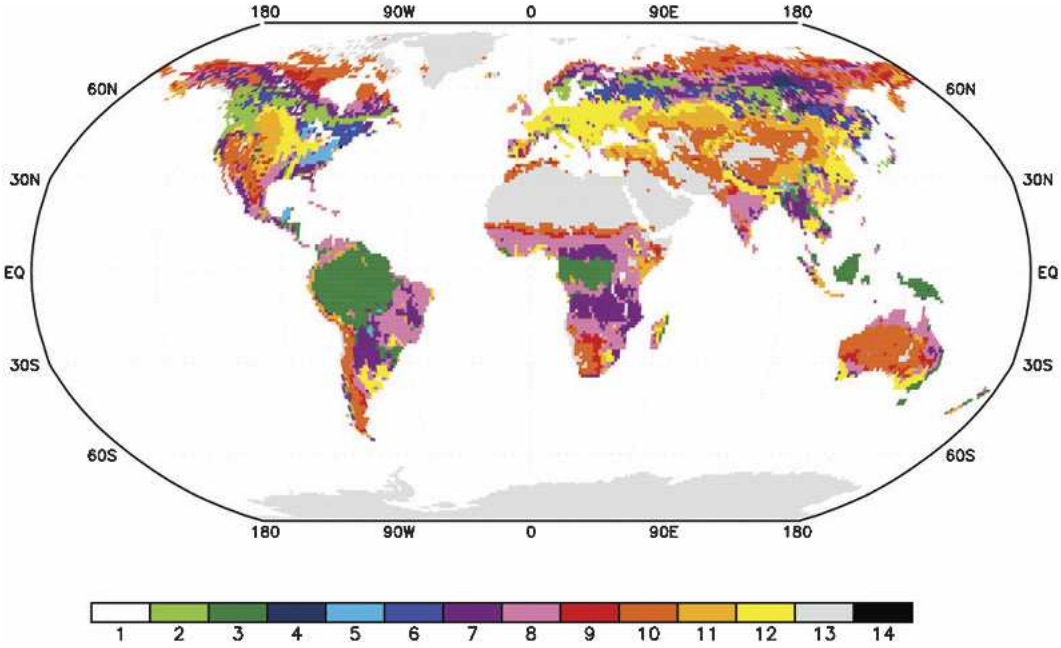

Figure 1. Predominant vegetation class in each 1° grid square: 1) water, 2) evergreen needle-leaf forest, 3) evergreen broadleaf forest, 4) deciduous needle-leaf forest, 5) deciduous broadleaf forest, 6) mixed forest, 7) woodland (40%–60% tree cover), 8) wooded grassland (10%–40% tree cover), 9) closed shrubland (>40% shrub cover), 10) open shrubland (10%–40% shrub cover), 11) grassland and cereal crops, 12) broadleaf crops, 13) barren or ice covered, and 14) urban.

$$\text{foliar\_C} = [(\text{LAI} \times \text{LAI\_F}) \times \text{SLA}^{-1}]; \quad (1)$$

$$\text{wood\_C} = [\text{wd\_fract} \times (\text{LAI\_MX} \times 1.25)]; \quad (2)$$

$$\text{veg\_water} = (\text{foliar\_C} \times 2.22 \times \text{foliar\_W}) + (\text{wood\_C} \times 2.22 \times \text{wood\_W}); \quad (3)$$

$$\text{TB} = (2.22 \times \text{foliar\_C}) + (2.22 \times \text{wood\_C}) + \text{veg\_water}; \quad (4)$$

where

foliar_C = foliar biomass (kg C m^{-2}),

wood_C = wood biomass (kg C m^{-2}),

wd_fract = estimated proportion of wood to foliar biomass within pixel (–),

LAI = leaf area index (one sided, m^2 m^{-2}),

LAI_F = ratio of all-sided to one-sided leaf area index (–),

LAI_MX = annual monthly maximum leaf area index (m^2 m^{-2}),

foliar_W = water content of foliar biomass expressed as a proportion of dry biomass (–),

SLA = canopy specific leaf area per unit biomass (m^2 kg C^{-1}),

wood_W = wood water content expressed as a proportion of dry biomass (–),

veg_water = total above-ground vegetation water content (kg m^{-2}), and

TB = total biomass (kg m^{-2}).

The primary inputs for (1), (2), and (3) are land-cover class and LAI; all other parameters are indexed to individual land-cover classes (Table 2). Equation (2) was derived from an empirical relationship between NDVI and above-stump woody biomass (Dong et al. 2003). This approach was originally developed from AVHRR NDVI and forest inventory data for boreal and temperate forests and has been modified for use with LAI inputs rather than NDVI, and to account for differences in woody biomass between forest and shrub land-cover classes. For (3) and (4) it was assumed that biomass is composed of 45% carbon (Reichle et al. 1973). The parameters LAI_F and SLA were obtained from the literature for major biomes as summarized by White et al. (White et al. 2000). The parameter wd_fract is an empirical scalar to account for differences in the slope of the LAI–woody biomass relationship between forests (e.g., Dong et al. 2003) and other cover types where woody material is less prevalent. The parameters leaf_W and wood_W were derived from the literature for general cover types as follows: forests (Saatchi and Moghaddam 2000; Odum and Pigeon 1970; Kozlowski 1968; Leckie and Ranson 1998), shrubland (Sternberg and Shoshany 2001), grassland and crops [the Southern Great Plains (SGP97) database: http://daac.gsfc.nasa.gov/CAMPAIGN_DOCS/SGP97/ai1.html.].

3. Computing the geodynamic effects

A surface mass density distribution $\sigma(\theta,\lambda)$ can be conveniently expanded into spherical harmonics, where the coefficients of the expansion are the multiples of

Table 2. Biophysical parameters of global land-cover classes for estimating vegetation water content and total biomass using Equations (1)–(4).

Land-cover class	LAI_F	SLA	Wd_fract	Foliar_W	Wood_W
1	0.0	0.0	0.0	0.0	0.0
2	2.6	8.2	1.0	0.681	1.0
3	2.0	32.0	1.0	2.34	1.0
4	2.0	22.0	1.0	1.95	1.0
5	2.0	32.0	1.0	1.95	1.0
6	2.3	20.0	1.0	1.31	1.0
7	2.0	40.0	0.5	1.86	1.0
8	2.1	30.0	0.25	1.30	0.54
9	2.3	12.0	0.12	0.82	0.54
10	2.3	12.0	0.06	0.82	0.54
11	2.0	49.0	0.0	1.78	NA
12	2.0	12.0	0.0	2.0	NA
13	2.3	12.0	0.0	0.82	NA
14	2.3	12.0	0.03	0.82	0.54

$\sigma(\theta,\lambda)$. It has been shown that the Stokes coefficient of the spherical harmonic component of the gravity field due to $\sigma(\theta,\lambda)$, for each degree and order, is proportional to this multipole (e.g., Chao 1994). Therefore, in the Eulerian description, the time-variable Stokes coefficients of degree ($l = 0, 1, 2, \ldots,$) and order ($m = -l, \ldots, l$) are given by

$$\Delta C_{lm}(t) + i\,\Delta S_{lm}(t) = \frac{(1+k_l')\,a^2}{(2l+1)M}\int\int \Delta\,\sigma(\theta,\lambda;t)\,P_{lm}(\cos\theta)\exp(im\lambda)\sin\theta\quad d\theta\quad d\lambda, \tag{5}$$

where the Legendre functions are 4π normalized. Equation (5) constitutes the time-variable gravity signal of biomass, and the integration is carried out over the land area. The amplitude is modified by the load Love number k_l'; for example, for $l = 2$, the factor $1 + k_l' = 0.69$, meaning that the net mass effect is reduced by 31% due to the elastic yielding of the solid Earth. This factor approaches 1 as l increases. Anticipating their appearance later, the conventional zonal J coefficients are defined as $J_l = -\sqrt{(2l+1)}C_{l0}$.

Multiplying the Stokes coefficients with Earth's radius a gives the corresponding geoid height change. In particular, the three $l = 1$ terms multiplied by a give the three components of the geocenter shift vector. Similarly, extending it to the $l = 0$ term ΔC_{00} and multiplying by Earth's mass M results in the total biomass variation. There is another correction necessary in order to ensure the mass conservation: biomass is exchanged with the ocean as its ultimate source and sink. A uniform change of sea level is assumed following the exchange, and this sea level change is accounted for by a similar integration as (5) over the ocean area. This "ocean correction" is usually is no more than a few percent of the total (Chao and O'Connor 1988).

Equation (5) also gives the "mass terms" of the angular momentum due, in this case, to biomass's change of the inertia tensor, which is directly related to Earth's rotation: the polar motion excitation Ψ (with the real part giving the x component along the Greenwich meridian and the imaginary part the y component along 90°E) is proportional to the second-degree, first-order Stokes coefficients: $\Psi = -\sqrt{(5/3)}\,[Ma^2/(C-A)]\,(\Delta C_{lm} + i\,\Delta S_{lm})$, whereas the excitation of the length-of-day (LOD) change ΔLOD is proportional to ΔC_{20}: $\Delta\text{LOD/LOD} = -2\sqrt{(5)}/3\,[(Ma^2/C)]\,\Delta C_{20}$, if the conservation of mass is ensured (as it is via the ocean correction). Here we have neglected the "motion terms" of the angular momentum (e.g., Munk and MacDonald 1960), which is justified in the present case because the actual transport of the biomass is relatively slow. Note that C and A are respectively the equatorial and axial moments of inertia of the mantle only (as opposed to the entire Earth), as the nonparticipation of the core in the Earth rotation excitation process is assumed at the time scales in question.

Summarized in Table 1, a more detailed description of the above formulation can be found in Chao (Chao 1994); the treatment is actually identical to that of Chao (Chao 1995) for artificial reservoirs that impound water mass on land. The geodynamic results obtained by integrating the biomass $\sigma(\theta, \lambda; t)$ from section 2 according to the above formulas are presented below.

4. Results and discussion

4.1. Global distribution and variability of biomass

The monthly climatology shown in Figure 2 summarizes the seasonal variability of biomass. Based on the computed 17-yr time series, the average vegetation density on the land surface was 5.93 kg m^{-2} (Figure 3), which is equivalent to 0.89 teratons of terrestrial vegetation globally. The global mean temporal range of vegetation density over the 17-yr period (mean, over all land points, of the 17-yr maximum minus minimum vegetation density) was 1.69 kg m^{-2} (Figure 4). The densest vegetation cover, approximately 36 kg m^{-2}, exists in the Amazon and parts of the boreal forests of Canada and central Asia. The seasonal progression of foliage from the southern peak in January toward its northern peak in July and August and back again is also apparent in Figure 2. The largest variability, roughly 5 kg m^{-2} between seasons on average, appears to occur in boreal forests. Of this, about 4 kg m^{-2} is attributable to changes in vegetation water storage. However, as noted later in the discussion of error sources (section 4.3.), some of the seasonal variability of remotely sensed LAI may be artificial, and because of the relatively small value of canopy specific leaf area (SLA) per unit of biomass assigned to evergreen needleleaf vegetation, small changes in LAI in the boreal forests yielded large changes in biomass. Tropical forests were determined to have little seasonal biomass variability, which is logical because they are evergreen. Interannual variations in biomass were generally small, except in eastern Australia and the deciduous needleleaf forests of northern Canada (Figure 5).

4.2. Contribution to global geodynamic effects and comparison with geodetic observations

Figures 6–8 show time series of low-degree gravity Stokes coefficients in terms of time-variable gravity, geocenter shifts, and Earth rotation variations, induced by the global biomass variation (see Table 1). For all time series, both seasonal (annual + semiannual + higher harmonics) and interannual variations are apparent, with no clear long-term secular trends during the period of study. Though larger than the interannual signal, the seasonal biomass signal is minor compared to other sources (see below). This does not diminish the importance of documenting it and thus refining our understanding of observed geodetic phenomena, particularly given the continuing improvement of monitoring techniques. The interannual anomalies are interesting; for example, they appear to have a slightly lagged correlation with the multivariate El Niño–Southern Oscillation (ENSO) index (not shown). The link between ENSO and large-scale vegetation characteristics is well known (e.g., Behrenfeld et al. 2001; Nemani et al. 2003); so the correlation is hardly surprising and will not be discussed here. The eruption of Mount Pinatubo on 15 June 1991 caused a decrease in net solar radiation around the world (Minnis et al. 1993), which impacted the growth of plants (e.g., Tucker et al. 2001). The resulting effects on Earth's orientation parameters can be seen in Figures 6–8, particularly in the C_{11} (Figure 6) and J_2 (Figure 7) time series.

4.2.1. Geocenter motion

The geocenter motion is of central importance in the definition of the terrestrial reference frame. Investigations have been conducted on the influence of mass

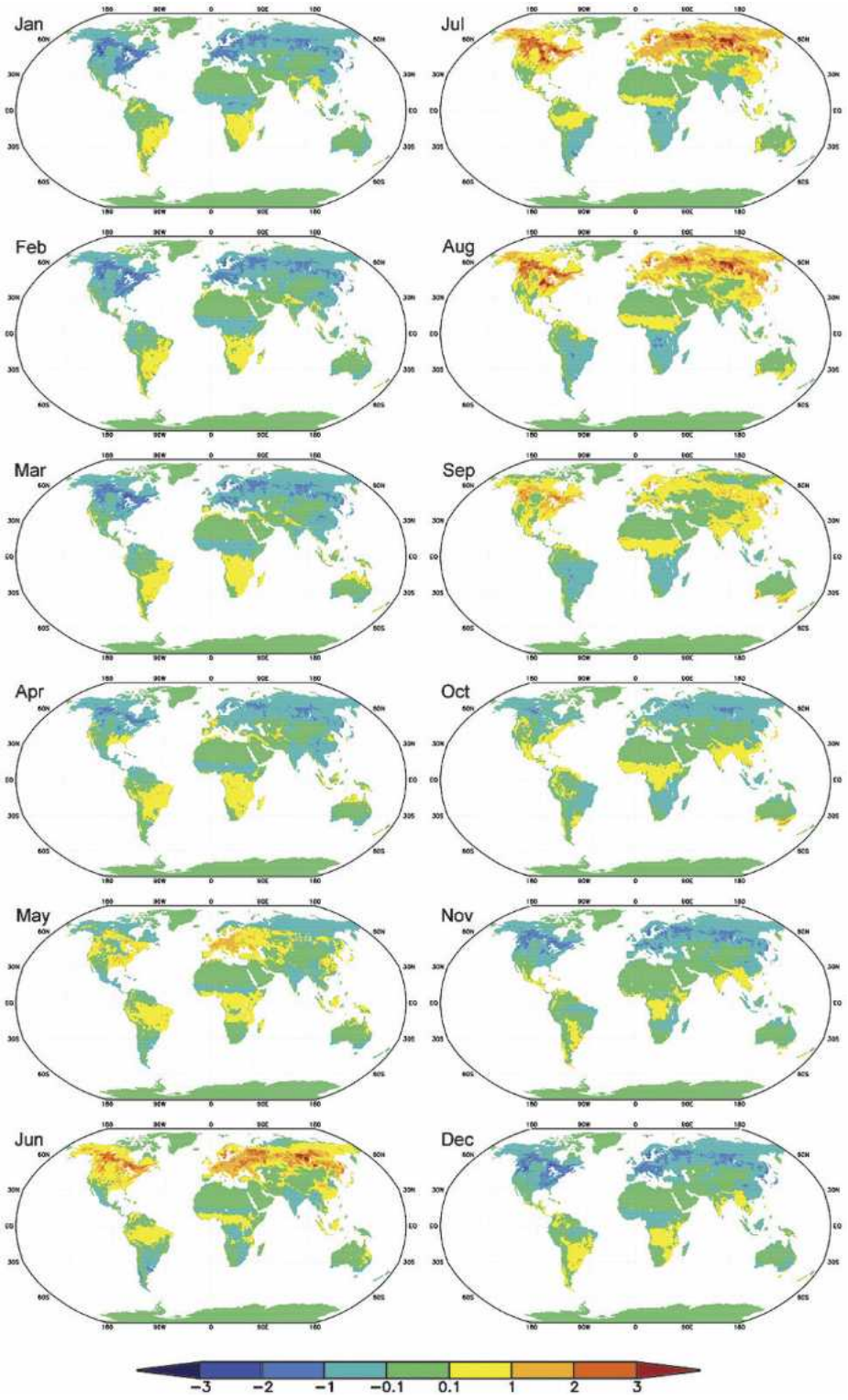

Figure 2. Climatology of biomass density (kg m^{-2}) as average anomalies for each month of the year.

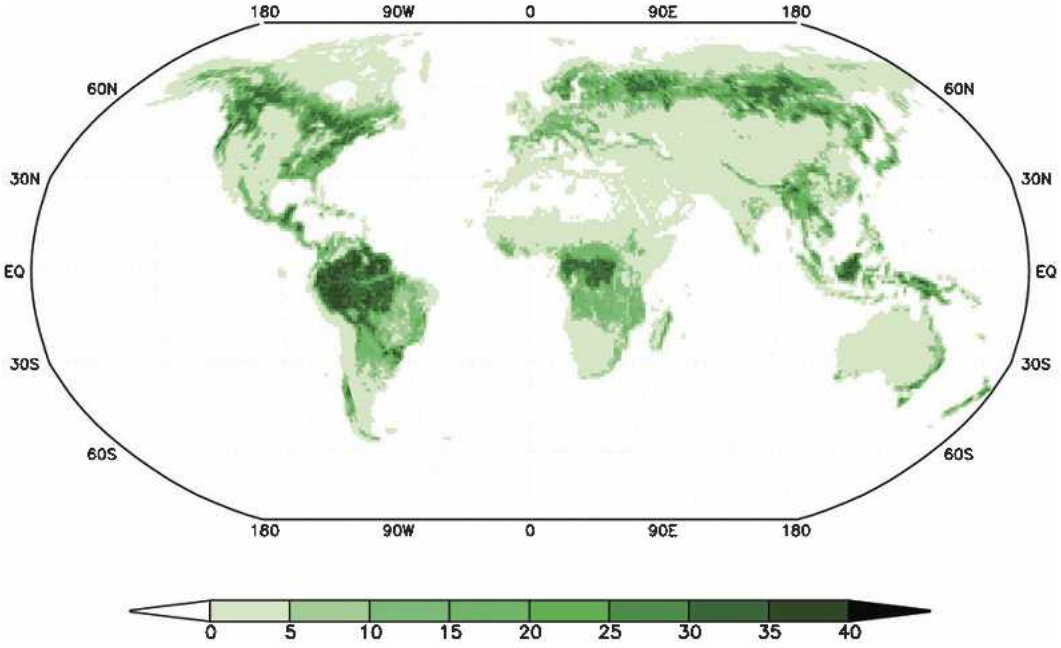

Figure 3. Mean biomass density (kg m^{-2}): 1982–98.

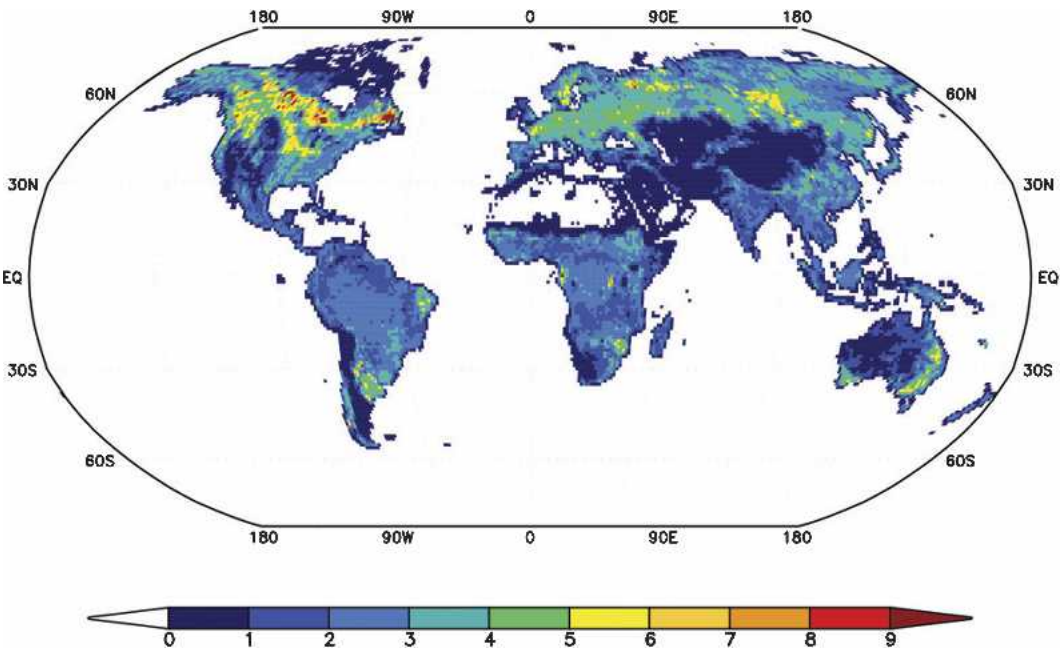

Figure 4. Range (maximum minus minimum) of biomass density (kg m^{-2}): 1982–98.

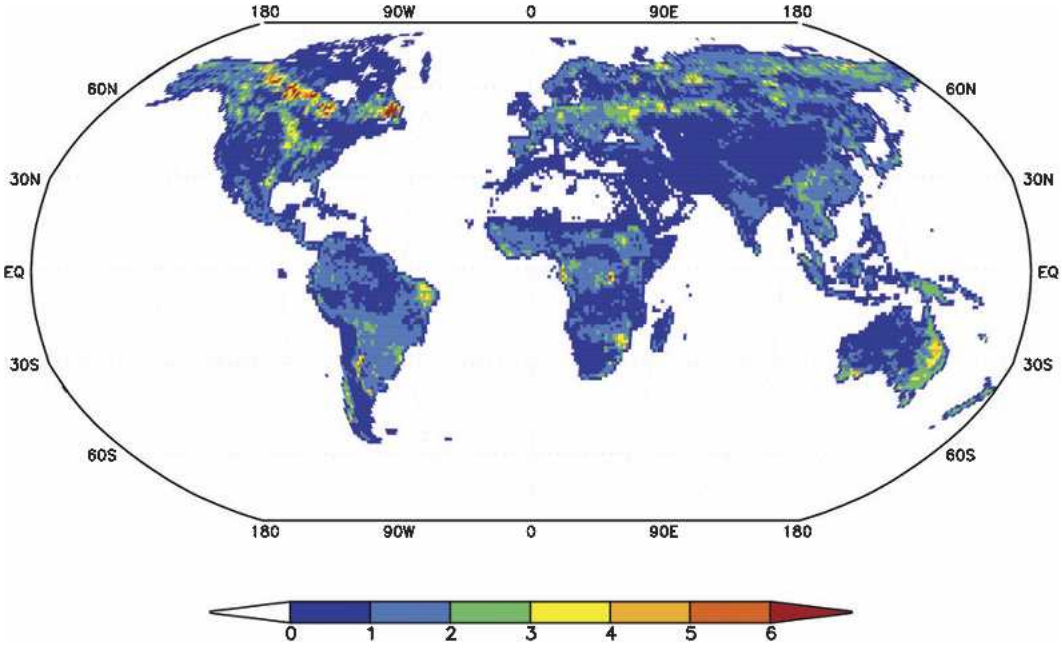

Figure 5. Range (maximum minus minimum) of biomass density (kg m^{-2}) over all the months of Jul from 1982–98.

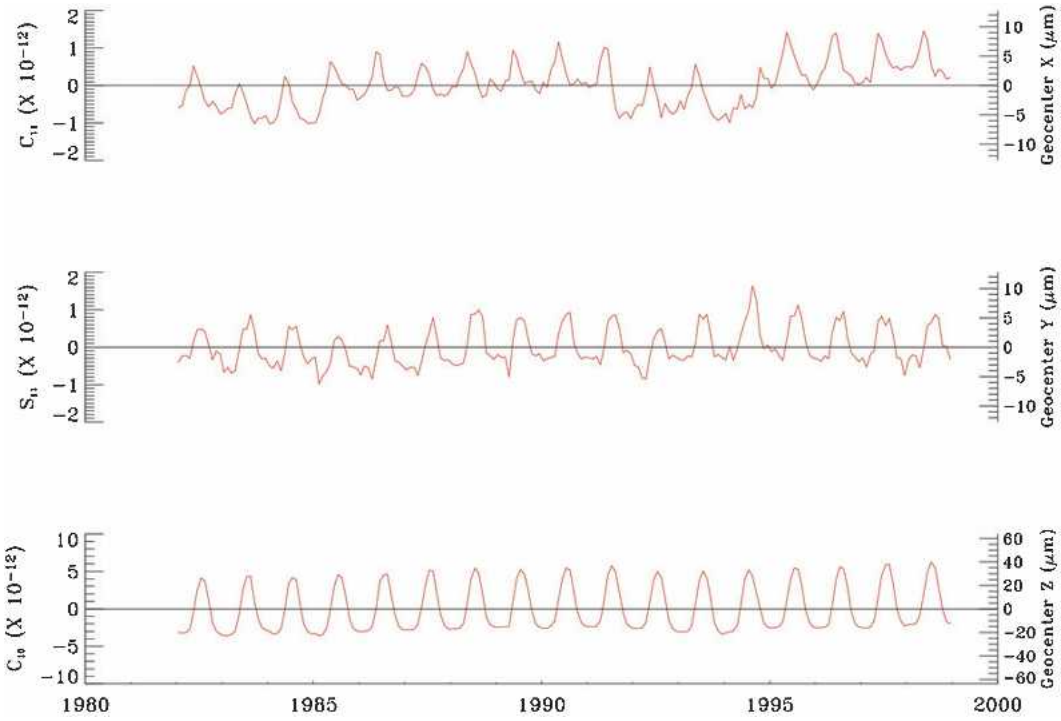

Figure 6. Global biomass gravity Stokes coefficients for $l = 1$ and the corresponding geocenter shift.

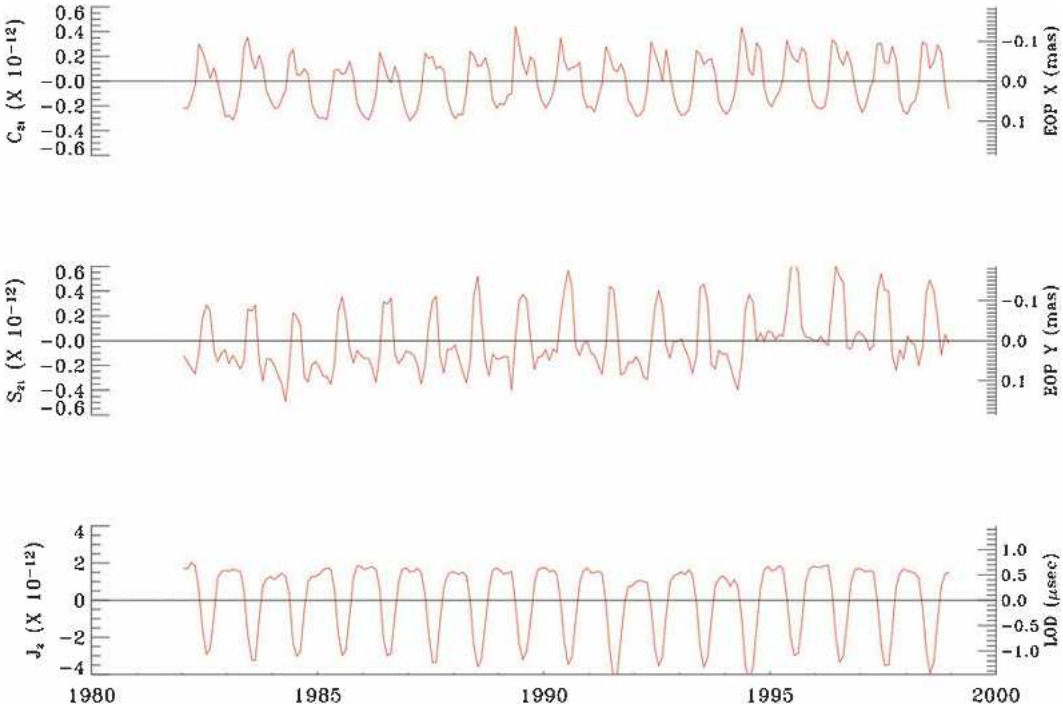

Figure 7. Global biomass gravity Stokes coefficients for $l = 2$ and the corresponding Earth orientation parameters.

redistribution of surface fluids (e.g., Dong et al., 1997) and the associated global deformation due to the seasonal mass loading (Blewitt et al. 2001). Figure 6 shows that the biomass-induced geocenter motion is on the order of several tens of micrometers, which is one to two orders of magnitude smaller than the contributions by other seasonal mass redistributions in the atmosphere and hydrosphere according to numerical models. Note that, as with the latter, the majority of the seasonal motion occurs in the north–south z direction, reflecting the hemispherical seasonality. Current monitoring of the geocenter from the space geodetic observations of satellite-laser ranging (e.g., Pavlis 2002) is insufficient to detect, or identify, this small motion.

4.2.2. Earth rotation variation

The contribution of biomass variability to seasonal polar motion, or the biomass excitation of the annual wobble, was determined to have an amplitude on the order of 0.1 mas (Figure 7). That is marginally detectable in today's measurement, for example, from the technique of very long baseline interferometry (e.g., Clark et al. 1998). The influence on the LOD is somewhat below current limits of detectability. In any case, like the geocenter motion, the biomass-induced signal in Earth's rotation excitation is obscured by contributions from various other sources in the atmosphere and hydrosphere, some of which are two orders of magnitude larger. The same is true for the interannual excitations.

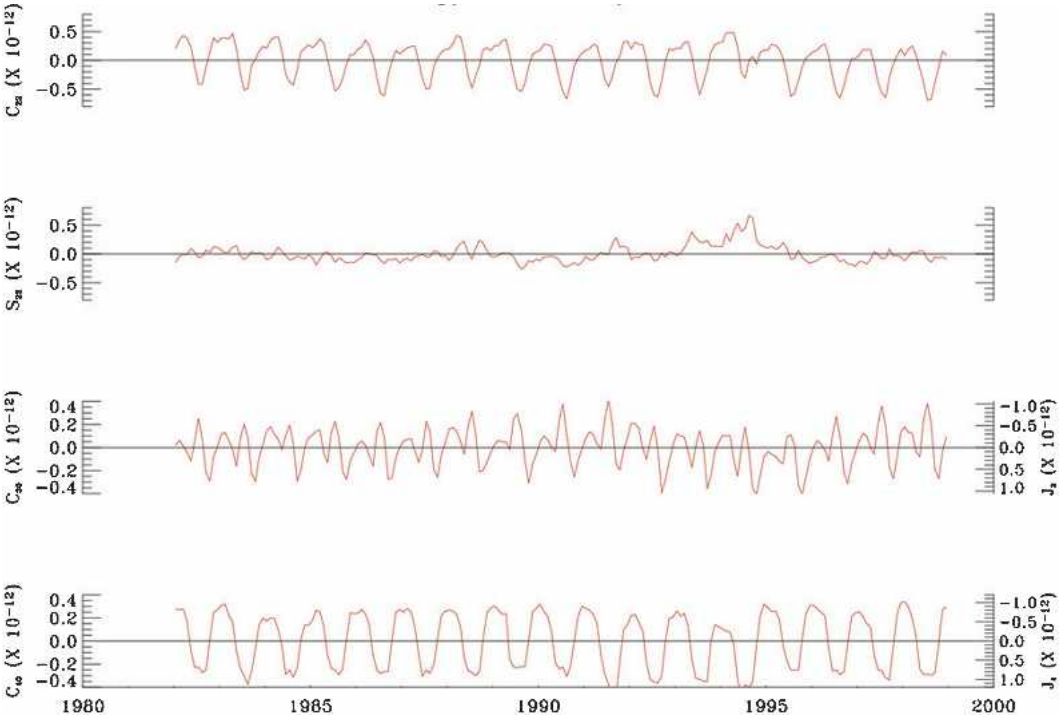

Figure 8. Global biomass Stokes coefficients for a few selected degrees and orders of magnitude.

4.2.3. Time-variable gravity

The satellite-laser-ranging technique has detected low-degree time-variable gravity due to various sources, particularly in J_2 (e.g., Cox and Chao 2002). Its measurement error, however, is an order of magnitude too large to detect the biomass-induced J_2 according to Figure 7, and even worse for the other low-degree Stokes coefficients, for example, those in Figure 8.

In March of 2002 the GRACE satellite mission was launched with the goal of producing a new model of Earth's gravity field every month for several years with high precision and spatial resolution (Tapley et al. 2004a). Based on analyses of modeled soil moisture and snow time series and the baseline error characteristics of the mission, Wahr et al. (Wahr et al. 1998) and Rodell and Famiglietti (Rodell and Famiglietti 1999) predicted that terrestrial water storage changes would be detectable by GRACE on monthly and longer time steps over regional to continental scales, depending on the magnitudes of the changes themselves. Terrestrial water storage changes are now being derived from GRACE observations (e.g., Wahr et al. 2004) and used in water cycle research (e.g., Rodell et al. 2004). However, disaggregating these changes vertically (i.e., into groundwater, soil moisture, snow, and the other components of terrestrial water storage) will require auxiliary observations and/or a more mature understanding of mass variability in the components (Rodell and Famiglietti 2001).

The results presented here contribute to our understanding of variability in one

of those components, vegetation, and we can now assess the sensitivity of GRACE to biomass variations. In terms of global harmonics, the gravitational effects of changes in biomass are predicted to be just sensible by GRACE at degrees 4–14 (Figure 9). However, more importantly, in certain regions seasonal biomass variations are on the same order as GRACE limits of detectability (Wahr et al. 2004), which is likely to improve as the retrieval algorithms mature (Tapley et al. 2004b). These regions include many parts of temperate North America and Eurasia. Hence, vegetation must be considered when attempting to explain or disaggregate the terrestrial mass changes and anomalies that are being derived from GRACE.

4.3. Sources of possible error

The LAI maps, the land-cover map, and the biophysical indices in Table 2 are based on parameters and assumptions that were upscaled or homogenized for global application. This simplification introduces uncertainty, because vegetation characteristics are variable in time and at subgrid scales, even within one species. Variability in the derived biomass maps is governed solely by variability of LAI. Regional estimation of biophysical variables such as LAI and biomass from global satellite remote sensing is a challenging task. Even for properly calibrated, clear-sky conditions, the relationship between surface spectral reflectance and LAI can

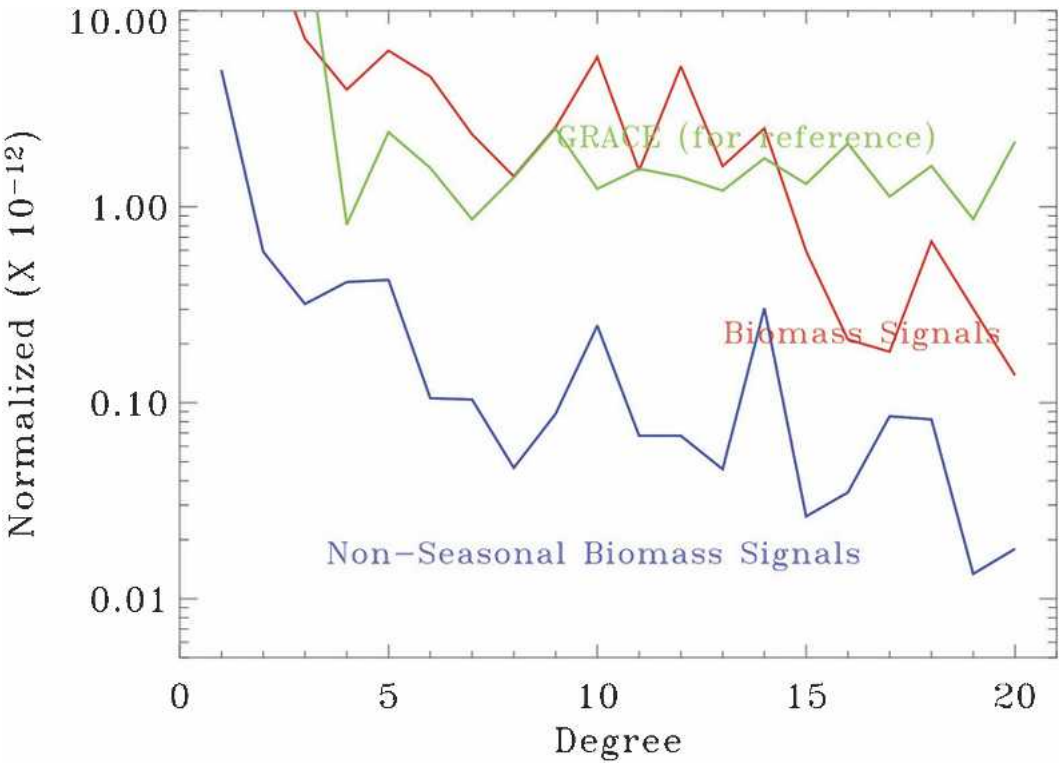

Figure 9. Comparison of estimated GRACE sensitivity with total and nonseasonal amplitude spectra of canopy mass.

vary independently of canopy cover depending on measurement geometry and surface characteristics such as snow cover and soil properties (Myneni et al. 1997). Areas such as tropical forests and boreal and arctic landscapes likely exhibit artificial seasonality in remotely sensed LAI due to the presence of considerable cloud cover and other atmospheric aerosol contamination for much of the year. Also, the relationship between satellite NDVI and LAI upon which these biomass estimates depend tends to be asymptotic, with saturation at LAI levels on the order of 3–5 (Turner et al. 1999) and biomass levels above 50–80 Mg ha^{-1}, depending upon vegetation type and structure (Dong et al. 2003). No attempt was made to account for spatial and temporal variability due to changes in general stand parameters within major biome types (i.e., Table 2). These parameters were derived from average values for general cover types and are likely highly variable within individual biomes (e.g., White et al. 2000). Actual biomass values are known to vary seasonally, diurnally, and spatially within individual vegetation classes. Canopy-averaged SLA (m^2 kg^{-1}) for example, describes the distribution of plant biomass relative to leaf area within a plant canopy and is an essential component of allocation models [e.g., Equation (1)]. General assumptions of constant SLA within major vegetation community types have been used extensively to facilitate comparisons between LAI and foliar biomass, and spatial extrapolation of general leaf trait relationships, vegetation productivity, and biomass attributes in remote sensing, allometric, and ecosystem model–based studies (e.g., Running and Hunt 1993; Running et al. 2000). While SLA is generally consistent within major plant functional types, it can also vary spatially and seasonally within a given biome according to changes in light regime and nitrogen availability, leaf longevity, and general climatic conditions (Pierce and Running 1994; Reich et al. 1999). Variability in SLA has been found to range from 19% to 44% within individual biome types, resulting in similar variability in biomass characteristics (White et al. 2000).

The NOAA satellites that carried the AVHRR instruments were serviced or replaced periodically between 1982 and 1998, which may have caused small but perceptible inconsistencies in the derived LAI fields, and hence the biomass estimates presented here. By comparing Figure 10, which displays NOAA satellite timelines for five land areas, with the Earth orientation parameter time series

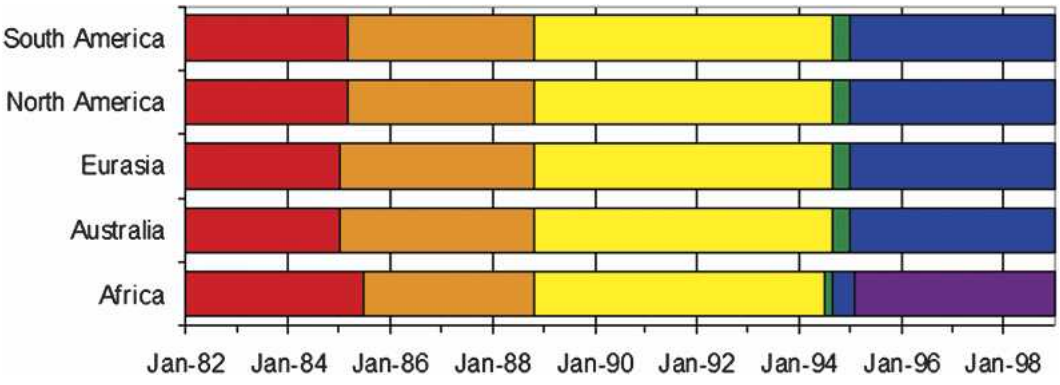

Figure 10. Timeline showing *NOAA-15* changes, which might have affected AVHRR-derived LAI, as color changes.

(Figures 6–8), artificial trends can be surmised. For example, the apparent adjustments in the $C_{1,1}$ time series (Figure 6) at the beginning of 1985 and the end of 1994 might not be real.

Errors in the estimated biomass fields are difficult to quantify due to a lack of independent, large-scale data for validation, but the results are generally consistent with the reported ranges of vegetation water content levels within major biomes (Leckie and Ranson 1998; Saatchi and Moghaddam 2000; Odum and Pigeon 1970; Jackson et al. 1999). Additionally, a recent comparison of these results with microwave optical thickness maps derived from mean monthly brightness temperature data from the Advanced Microwave Scanning Radiometer for EOS (AMSR-E) on board the NASA *Aqua* satellite yielded similar spatial patterns and general relationships among global land-cover class, microwave optical thickness, and vegetation water content (E. Njoku, Jet Propulsion Laboratory, California Institute of Technology, 2003, personal communication).

5. Summary

Global maps of vegetation biomass were produced for each month from January 1982 to December 1998 by applying field-based relationships to AVHRR measurements of LAI and vegetation type. These maps were used to compute geodetic anomalies, which in turn were compared with existing data on Earth's rotation variations, geocenter motion, and time-variable gravity, including the current accuracy of GRACE-derived terrestrial mass changes. It was determined that the seasonal amplitude of biomass far exceeds the interannual variability, reaching 5 kg m^{-2} in certain regions. The interannual signatures of ENSO and the 1991 eruption of Mount Pinatubo are nevertheless recognizable in the biomass-induced geodynamic signals. The seasonal geodetic anomalies are still one to two orders of magnitude smaller than those resulting from atmospheric and other terrestrial hydrological processes. The biomass variability is at or above GRACE's limits of detectability globally for harmonic degrees 4–14 and possibly, with expected future improvements in the retrieval algorithms, over certain regions including parts of temperate North America and Eurasia. Compared with other modern precise space geodetic measurements, the seasonal amplitudes are marginally detectable or one order of magnitude too small to be detected or identified. The biomass contributions, especially in the cases where they are detectable albeit marginally, should be considered and modeled in order to achieve a complete understanding and interpretation of the observational data.

Acknowledgments. We wish to thank Jon Gottschalck for his assistance in preparing the LAI data.

References

Behrenfeld, M. J., and Coauthors, 2001: Biospheric primary production during an ENSO transition. *Science,* **291,** 2594–2597.

Blewitt, G., D. Lavallee, P. Clarke, and K. Nurutdinov, 2001: A new global mode of Earth deformation: Seasonal cycle detected. *Science,* **294,** 342–345.

Chao, B. F., 1994: The Geoid and Earth Rotation. *Geophysical Interpretations of the Geoid*, P. Vanicek and N. Christou, Eds., CRC Press, 285–298.

——, 1995: Anthropogenic impact on global geodynamics due to water impoundment in major reservoirs. *Geophys. Res. Lett.,* **22,** 3529–3532.

——, and W. P. O'Connor, 1988: Effect of a uniform sea level change on the Earth's rotation and gravitational field. *Geophys. J.,* **93,** 191–193.

——, V. Dehant, R. S. Gross, R. D. Ray, D. A. Salstein, M. M. Watkins, and C. R. Wilson, 2000: Space geodesy monitors mass transports in global geophysical fluids. *Eos, Trans. Amer. Geophys. Union,* **81,** 247–250.

Clark, T. A., and Coauthors, 1998: Earth rotation measurement yields valuable information about the dynamics of the Earth system. *Eos, Trans. Amer. Geophys. Union*, **79**, 205–216.

Cox, C., and B. F. Chao, 2002: Detection of large-scale mass redistribution in the terrestrial system since 1998. *Science,* **297,** 831–833.

Dong, D., J. O. Dickey, Y. Chao, and M. K. Cheng, 1997: Geocenter variations caused by atmosphere, ocean, and surface ground water. *Geophys. Res. Lett.,* **24,** 1867–1870.

Dong, J., and Coauthors, 2003: Remote sensing estimates of boreal and temperate forest woody biomass: Carbon pools, sources and sinks. *Remote Sens. Environ.,* **84,** 393–410.

Gross, R., 2000: The excitation of the Chandler wobble. *Geophys. Res. Lett.,* **27** (15), 2329–2332.

Hansen, M. C., R. S. DeFries, J. R. G. Townshend, and R. Sohlberg, 2000: Global land cover classification at 1km spatial resolution using a classification tree approach. *Int. J. Remote Sens.,* **21,** 1331–1364.

Jackson, T. J., D. M. Le Vine, A. Y. Hsu, A. Oldak, P. J. Starks, C. T. Swift, J. D. Isham, and M. Haken, 1999: Soil moisture mapping at regional scales using microwave radiometry: The Southern Great Plains Hydrology Experiment. *IEEE Trans. Geosci. Remote Sens.,* **37,** 2136–2115.

Jeffreys, H., 1916: Causes contributory to the annual variation of latitude monthly notice. *Roy. Astron. Soc.,* **76,** 499.

Kozlowski, T. T., 1968: Introduction. *Water Deficits and Plant Growth*, T. T. Kozlowski, Ed., Vol. 1, Academic Press, 333 pp.

Kuehne, J., and C. R. Wilson, 1991: Terrestrial water storage and polar motion. *J. Geophys. Res.,* **96,** 4337–4345.

Leckie, D. G., and K. J. Ranson, 1998: Forestry applications using imaging radar. *Principles and Applications of Imaging Radar,* F. M. Henderson and A. J. Lewis, Eds., John Wiley and Sons, 435–509.

Minnis, P., E. F. Harrison, L. L. Stowe, G. G. Gibson, F. M. Denn, D. R. Doelling, and W. L. Smith, 1993: Radiative climate forcing by the Mount Pinatubo eruption. *Science,* **259,** 1411–1415.

Munk, W. H., and G. J. F. MacDonald, 1960: *The Rotation of the Earth*. Cambridge University Press, 323 pp.

Myneni, R. B., R. R. Nemani, and S. W. Running, 1997: Algorithm for the estimation of global land cover, LAI and FPAR based on radiative transfer models. *IEEE Trans. Geosci. Remote Sens.,* **35,** 1380–1393.

Nemani, R. R., and S. W. Running, 1997: Land cover characterization using multitemporal red, near-IR and thermal-IR data from NOAA/AVHRR. *Ecol. Appl.,* **7,** 79–90.

——, C. D. Keeling, H. Hashimoto, W. M. Jolly, S. C. Piper, C. J. Tucker, R. B. Myneni, and S. W. Running, 2003: Climate-driven increases in global terrestrial net primary production from 1982 to 1999. *Science,* **300,** 1560–1563.

Nerem, R. S., B. F. Chao, A. Y. Au, J. C. Chan, S. M. Klosko, N. K. Pavlis, and R. G. Williamson, 1993: Temporal variations of Earth's gravitational field from satellite laser ranging to LAGEOS. *Geophys. Res. Lett.,* **20,** 595–598.

Odum, H. T., and R. F. Pigeon, Eds., 1970: *A Tropical Rainforest: A Study of Irradiation and Ecology at El Verde, Puerto Rico.* U.S. Atomic Energy Commission, National Technical Information Service, 1678 pp.

Pavlis, E. C., 2002: Dynamical determination of origin and scale in the Earth system from satellite laser ranging. *Proc. 2001 IAG Scientific Assembly,* Budapest, Hungary, IAG, 36–41.

Pierce, L. L., and S. W. Running, 1994: Regional-scale relationships of leaf area index to specific leaf area and leaf nitrogen content. *Ecol. Appl.,* **4** (2), 313–321.

Reich, P. B., D. S. Ellsworth, M. B. Walters, J. M. Vose, C. Gresham, J. C. Volin, and W. D. Bowman, 1999: Generality of leaf trait relationships: A test across six biomes. *Ecology,* **80** (6), 1955–1969.

Reichle, D. E., B. E. Dinger, N. T. Edwards, W. F. Harris, and P. Sollins, 1973: Carbon flow and storage in a forest ecosystem. *Carbon and the Biosphere,* G. M. Woodwell and E. V. Pecan, Eds., National Technical Information Service, 345–365.

Riley, G., 1944: The carbon metabolism and photosynthetic efficiency of the Earth as a whole. *Amer. Sci.,* **32,** 129.

Rodell, M., and J. S. Famiglietti, 1999: Detectability of variations in continental water storage from satellite observations of the time dependent gravity field. *Water Resour. Res.,* **35,** 2705–2723.

——, and ——, 2001: An analysis of terrestrial water storage variations in Illinois with implications for the Gravity Recovery and Climate Experiment (GRACE). *Water Resour. Res.,* **37,** 1327–1340.

——, ——, J. Chen, S. Seneviratne, P. Viterbo, S. Holl, and C. R. Wilson, 2004: Basin scale estimates of evapotranspiration using GRACE and other observations. *Geophys. Res. Lett.,* **31,** L20504, doi:10.1029/2004GL020873.

Running, S. W., and E. R. Hunt, 1993: Generalization of a forest ecosystem process model for other biomes, BIOME-BGC, and an application for global-scale models. *Scaling Physiological Processes: Leaf to Globe,* J. R. Ehleringer and C.B. Field, Eds., Academic Press, 141–158.

——, P. E. Thornton, R. Nemani, and J. M. Glassy, 2000: Global terrestrial gross and net primary productivity from the Earth Observing System. *Methods in Ecosystem Science,* O. Sala, R. Jackson, and H. Mooney, Eds. Springer-Verlag, 44–57.

Saatchi, S. S., and M. Moghaddam, 2000: Estimation of crown and stem water content and biomass of boreal forest using polarimetric SAR imagery. *IEEE Trans. Geosci. Remote Sens.,* **38** (2), 697–709.

Smith, D. E., and D. L. Turcotte, Eds., 1993:*Contributions of Space Geodesy to Geodynamics.* Geodynamics Series, Vols. 23–25, Amer. Geophys. Union, 861 pp.

Sternberg, M., and M. Shoshany, 2001: Above ground biomass allocation and water content relationships in Mediterranean trees and shrubs in two climatological regions in Israel. *Plant Ecol.,* **157,** 171–179.

Tapley, B., S. Bettadpur, M. Watkins, and C. Reigber, 2004a: The gravity recovery and climate experiment: Mission overview and early results. *Geophys. Res. Lett.,* **31**, L09607, doi: 10.1029/2004GL019920.

——, S. Bettadpur, J. C. Ries, P. F. Thompson, and M. M. Watkins, 2004b: GRACE measurements of mass variability in the Earth system. *Science,* **305,** 503–505.

Tucker, C. J., D. A. Slayback, J. E. Pinzon, S. O. Los, R. B. Myneni, and M. G. Taylor, 2001: Higher northern latitude normalized difference vegetation index and growing season trends from 1982 to 1999. *Int. J. Biometeor.,* **45,** 184–190.

Turner, D. P., W. B. Cohen, R. E. Kennedy, K. S. Fassnacht, and J. M. Briggs, 1999: Relationships between leaf area index and Landsat TM spectral vegetation indices across three temperate zone sites. *Remote Sens. Environ.,* **70,** 52–68.

Wahr, J., M. Molenaar, and F. Bryan, 1998: Time-variability of the Earth's gravity field: Hydrological and oceanic effects and their possible detection using GRACE. *J. Geophys. Res.,* **103** (B12), 30 205–30 230.

——, S. Swenson, V. Zlotnicki, and I. Velicogna, 2004: Time-variable gravity from GRACE: First results. *Geophys. Res. Lett.,* **31,** L11501, doi:10.1029/2004GL019779.

White, M. A., P. E. Thornton, S. W. Running, and R. R. Nemani, 2000: Parameterization and sensitivity analysis of the BIOME-BGC terrestrial ecosystem model: Net primary production controls. *Earth Interactions,* **4**. [Available online at http://EarthInteractions.org.]